

A Fluorescence Sensor Array Based on Zinc(II)-Carboxyamidoquinolines: Toward Quantitative Detection of ATP**

Mariia Pushina,^[a] Sepideh Farshbaf,^[a] Wakana Mochida,^[b] Masashi Kanakubo,^[b] Ryuhei Nishiyabu,^[b] Yuji Kubo,^{*,[b]} and Pavel Anzenbacher, Jr.^{*,[a]}

Abstract: The newly prepared fluorescent carboxyamidoquinolines (1–3) and their Zn(II) complexes (Zn@1–Zn@3) were used to bind and sense various phosphate anions utilizing a relay mechanism, in which the Zn(II) ion migrates from the Zn@1–Zn@3 complexes to the phosphate, namely adenosine 5'-triphosphate (ATP) and pyrophosphate (PPi), a process accompanied by a dramatic change in fluorescence. Zn@1–Zn@3 assemblies interact with adenine nucleotide phosphates while displaying an analyte-specific response. This process was investigated using UV-vis, fluorescence, and NMR spectroscopy. It is shown that the different binding selectivity and the corresponding fluorescence response enable differ-

entiation of adenosine 5'-triphosphate (ATP), adenosine 5'-diphosphate (ADP), pyrophosphate (PPi), and phosphate (Pi). The cross-reactive nature of the carboxyamidoquinolines-Zn(II) sensors in conjunction with linear discriminant analysis (LDA) was utilized in a simple fluorescence chemosensor array that allows for the identification of ATP, ADP, PPi, and Pi from 8 other anions including adenosine 5'-monophosphate (AMP) with 100% correct classification. Furthermore, the support vector machine algorithm, a machine learning method, allowed for highly accurate quantitation of ATP in the range of 5–100 μM concentration in unknown samples with error < 2.5%.

Introduction

Recognition^[1] and sensing^[2] of phosphate-related anions is an important area of research due to their biological and environmental functions, whether in cellular energy transduction and transfer of genetic information,^[3] protein synthesis,^[4] pH and osmotic pressure regulation,^[5] or many others.^[6] Inorganic phosphates have enormous application in industry as both raw materials and fertilizers responsible for anthropogenic eutrophication.^[7] Here, a particular attention has been devoted to sensing of biological phosphates such as pyrophosphate and adenosine phosphates, namely adenosine 5'-triphosphate (ATP), which plays a central role in biological processes. Also, illnesses such as kidney diseases, cardiovascular diseases, Parkinson's, Alzheimer's, and hypoglycemia are associated with large deviations of ATP levels.^[8] Therefore, the quantitation of ATP

could provide a way to diagnosis of such ailments. Among the methods used for the detection of ATP are those such as HPLC^[9] and enzyme-based analyses,^[10] which are still costly and require specialized labs.

More recently, chemosensors that utilize changes in their optical properties for signaling allowing for the implementation of simple analytical procedures came to the fore,^[11] and a significant effort has been devoted to improving the recognition of ATP with optical sensors.^[12] Such sensors frequently display cross-reactive responses to other phosphate ions such as adenosine 5'-diphosphate (ADP), adenosine 5'-monophosphate (AMP), pyrophosphate (PPi), and phosphate (Pi), and may thus be employed in simultaneous detection and discrimination of phosphate analytes. Sensor arrays comprising few cross-reactive sensors utilize fingerprint-like response patterns specific for an analyte and/or analyte concentration to achieve classification as well as the quantification. Such array sensors are frequently aided by pattern recognition techniques to accomplish the analyte classification and quantification.^[13] Thus, various chemosensor arrays have been developed and used for the detection of nucleotides,^[14] saccharides,^[15] peptides,^[16] proteins,^[17] metal ions,^[18] and other organic^[19] and inorganic^[20] analytes. However, few chemosensor arrays were established for the quantitation of triphosphates such as ATP.^[21] To the best of our knowledge, chemosensor arrays capable of the quantitation of ATP at less than 0.1 mM levels have not yet been developed despite the obvious appeal of such sensitive arrays, for example, in the quantitative measurement of trace ATP levels in biological fluids where ATP frequently appears at micromolar concentration. To address this issue, we have

[a] Dr. M. Pushina, S. Farshbaf, Prof. Dr. P. Anzenbacher, Jr.
Department of Chemistry
Bowling Green State University
Bowling Green, OH, 43403 (USA)
E-mail: pavel@bgsu.edu

[b] W. Mochida, M. Kanakubo, Dr. R. Nishiyabu, Prof. Dr. Y. Kubo
Department of Applied Chemistry
Graduate School of Urban Environmental Sciences
Tokyo Metropolitan University
Tokyo 192-0397 (Japan)
E-mail: yujik@tmu.ac.jp

[**] ATP = adenosine 5'-triphosphate.

 Supporting information for this article is available on the WWW under <https://doi.org/10.1002/chem.202100896>

prepared fluorescence-based sensors that display high selectivity and sensitivity for phosphates and can operate in aqueous solutions of analytes.

Results and Discussion

Synthesis of carboxyamidoquinoline ligands (1–3)

To obtain fluorescent complexes with zinc(II), we used an aminoquinoline cleft-type ligand as this and similar moieties exhibit enhanced fluorescence upon binding to zinc(II).^[22] Carboxyamidoquinoline (1) (Figure 1) was synthesized through Schiff base formation of salicylaldehyde with 2-amino-*N*-(quinolin-8-yl)acetamide and the following reductive amination reaction. The hydroxy group of 1 serves as an additional coordination site for zinc(II). A carboxyamidoquinoline with a 2-(2-benzothiazolyl)phenol moiety (2) was then synthesized from 3-(benzo[*d*]thiazol-2-yl)-2-hydroxy-5-methylbenzaldehyde and 2-amino-*N*-(quinolin-8-yl)acetamide. In addition, compound 3, an intermediate in the synthesis of 2 was also isolated and used as a fluorescent sensor ensemble with zinc(II). The assignment of 1–3 was carried out using ¹H NMR, ¹³C NMR, MS, and elemental analysis (Figure 1).

The absorption spectra of 1 recorded in a 4-(2-hydroxyethyl)-1-piperazineethanesulfonic acid (HEPES) buffer solution (10 mM, pH=7.0) containing acetonitrile (50%, v/v) and 1 (5.0 μM) show an absorption band at 310 nm and the

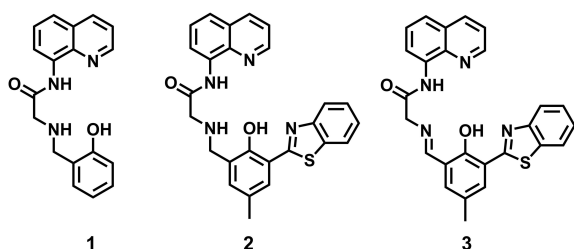


Figure 1. Structures of carboxyamidoquinoline-based ligands (1–3).

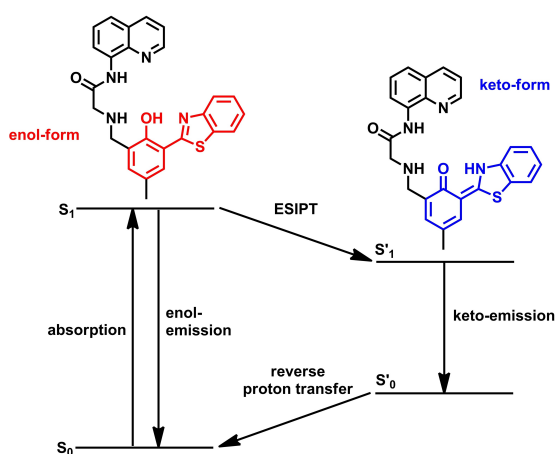


Figure 2. ESIP process taking place in 2.

corresponding fluorescence band at 410 nm assigned to the amidoquinoline moiety (Figure S12).^[23] In contrast to 1, absorption spectra of 2 and 3 are dominated by the bands characteristic of the hydroxyphenyl benzothiazole moieties (Figure S13 and S14). This is due to the high extinction coefficient of the hydroxyphenyl benzothiazole moiety compared to that of the amidoquinoline. In addition to emission bands at ca. 471 nm from the enol form, 2 and 3 also show emission bands at ca. 550 nm corresponding to the keto forms generated by the excited state intramolecular proton transfer (ESIPT) process (Figure 2).^[24]

An important part of the sensor design is the signal transduction. To recognize and sense phosphate ions, we focused on a fluorescent metal complexes of 1–3 capable of forming a chelate with the phenolate moiety and the nitrogens of the 2-amino-*N*-(quinolin-8-yl)acetamide moiety. We have tested several metal ions. Figure 3 shows that among the various metal ions, only zinc(II) provides high fluorescence response and was therefore used in further experiments.

Preparation of fluorescent ensembles of 1–3 with zinc(II) ions

To determine the conditions for preparation of the ensembles with zinc(II), fluorescence titrations of 1–3 with zinc(II) nitrate were performed in a HEPES buffer solution (10 mM, pH=7.0) containing acetonitrile (50%, v/v). The addition of zinc(II) led to significant spectral changes in 1–3 (Figure 4). The spectral changes and the resulting isotherms clearly showed the saturation of the changes upon addition of one equivalent of zinc(II). These data as well as Job's plots indicate 1:1 stoichiometry of the complexes (Figures S16–S18). This is further supported by the ESI-MS spectrometry also showing the complexes at 1:1 stoichiometry for 1–3 with zinc(II). The association constants for the formation of the ensembles Zn@1–Zn@3 derived from non-linear curve fitting of the corresponding isotherms were determined to be $(8.0 \pm 0.7) \times 10^6 \text{ M}^{-1}$, $(2.4 \pm 1.0) \times 10^7 \text{ M}^{-1}$, and $(7.4 \pm 1.1) \times 10^7 \text{ M}^{-1}$, respectively. Additionally, the UV-vis absorption titrations of 1–3 with zinc(II) also support the proposed binding modes (Figures S22–S24).

The observed spectral behavior also provides structural information about the resulting ensembles. Upon the formation

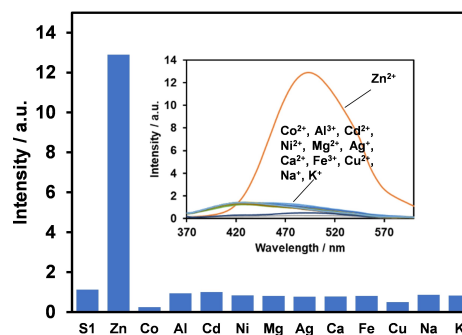


Figure 3. Fluorescence spectra of 1 (20 μM) and different metal ions (20 μM) in DMSO:HEPES buffer (pH=7.0) = 3:97 (v:v) at 25 °C; λ_{ex} = 365 nm.

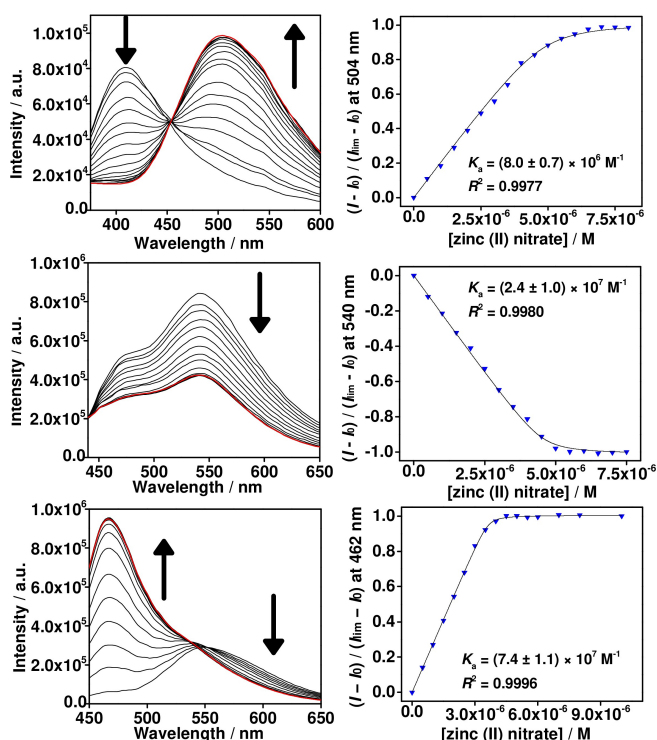


Figure 4. Top: Fluorescence titration spectra of **1** (5.0 μM) upon addition of incremental amounts of zinc(II) nitrate ($\lambda_{\text{ex}} = 330 \text{ nm}$). Middle: Fluorescence titration spectra of **2** (5.0 μM) upon addition of incremental amounts of zinc(II) nitrate ($\lambda_{\text{ex}} = 345 \text{ nm}$). Bottom: Fluorescence titration spectra of **3** (5.0 μM) upon addition of incremental amounts of zinc(II) nitrate ($\lambda_{\text{ex}} = 435 \text{ nm}$). All titrations were performed in HEPES buffer solutions (10 mM, pH = 7.0) containing acetonitrile (50%, v/v).

of **Zn@1**, the emission intensity at 410 nm gradually decreases with simultaneous appearance of a new emission peak at 504 nm (Figure 4 Top). The enhanced emission with the significant bathochromic shift of 94 nm can be attributed to the intramolecular charge transfer (ICT) from deprotonated 8-amido group to the quinoline moiety.^[25]

The addition of zinc(II) to **2** led to the decrease in the fluorescence intensities of both emission bands from both the keto and enol forms (Figure 4 center). This decrease can be attributed to the coordination of phenolic oxygen atom of **2** with zinc(II) ions as this binding promotes the deprotonation of the phenolic hydroxy group, which enhances the thermal deactivation of the excited state by the free rotation of the benzothiazole moiety. The increase in the proportion of the fluorescence from the enol during the fluorescence titrations also supports the proposed binding mode as the binding of the oxygen atom to zinc(II) ions prevents the ES IPT processes from taking place (Figure S26).^[26]

In contrast to **2**, a fluorescence enhancement of the emission band from the enol form was detected as a result of the 1:1 stoichiometric complexation of **3** with zinc(II) (Figure 4). The enhanced fluorescence of **3@Zn** could be interpreted by the coordination of the phenolate oxygen and the imine nitrogen of **3** to zinc(II) where the former inhibits the ES IPT processes and the latter prevents the photo-induced electron

transfer (PET) from the lone pair electron of the imine nitrogen to the excited state of the 2-(2-hydroxyphenyl)benzothiazole moiety (Figure S27).^[27]

To obtain further information regarding the structure of the complexes, ¹H NMR experiments with zinc(II) were performed in DMSO-*d*₆/D₂O (3:1 (v:v), 20 mM HEPES, pD = 7) (Figure 5–7). The addition of zinc(II) led to significant changes in the chemical shifts of the proton signals of the phenolic benzene ring as well as the quinoline ring of **1**, indicating the participation of the phenolic oxygen atom as an additional coordination site for the complexation (Figure 5 and S25).^[28]

¹H NMR titration experiment provides further structural information regarding the structure of **Zn@2**. The addition of zinc(II) to **2** led to negligible shifts of the proton signals of the benzothiazole ring while dramatic shifts of the proton signals of the quinoline ring as well as the benzene ring were observed. These shifts indicate the absence of the interaction between the nitrogen atom of the benzothiazole ring and zinc(II) ion as well as the participation of the phenolic oxygen and the nitrogen of the quinoline moiety in the coordination to zinc(II) (Figure 6 and S26). Similar behavior was observed in the case of **3** (Figure 7, S27, and S44).

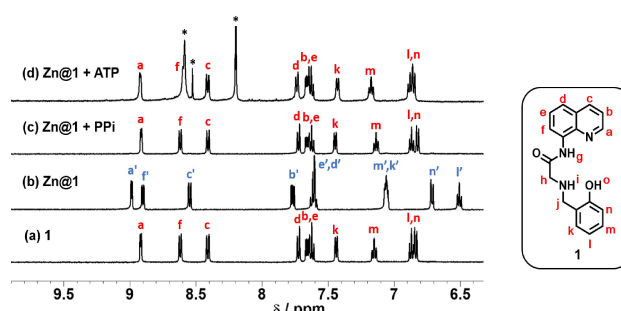


Figure 5. ¹H NMR spectra of **1** in the absence (a) and in the presence of zinc(II) ion (b). ¹H NMR spectra of **1** in the presence of zinc(II) upon addition of PPi (c) and ATP (d). Conditions: [**1**] = 1.00 mM, [zinc(II)] = 1.25 mM, [PPi] = 2.00 mM, [ATP] = 2.00 mM in DMSO-*d*₆: HEPES (20 mM, pD = 7) = 3:1 (v:v). The signals marked with asterisks denote the signals of ATP.

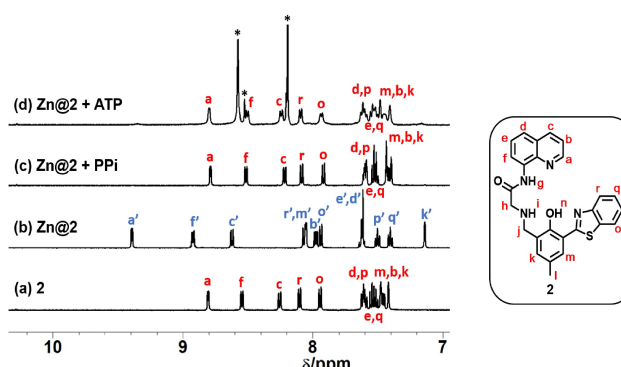


Figure 6. ¹H NMR spectra of **2** in the absence (a) and in the presence of zinc(II) ion (b). ¹H NMR spectra of **2** in the presence of zinc(II) upon addition of PPi (c) and ATP (d). Conditions: [**2**] = 1.00 mM, [zinc(II)] = 1.25 mM, [PPi] = 3.00 mM, [ATP] = 3.00 mM in DMSO-*d*₆: HEPES (20 mM, pD = 7) = 3:1 (v:v). The signals marked with asterisks denote the signals of ATP.

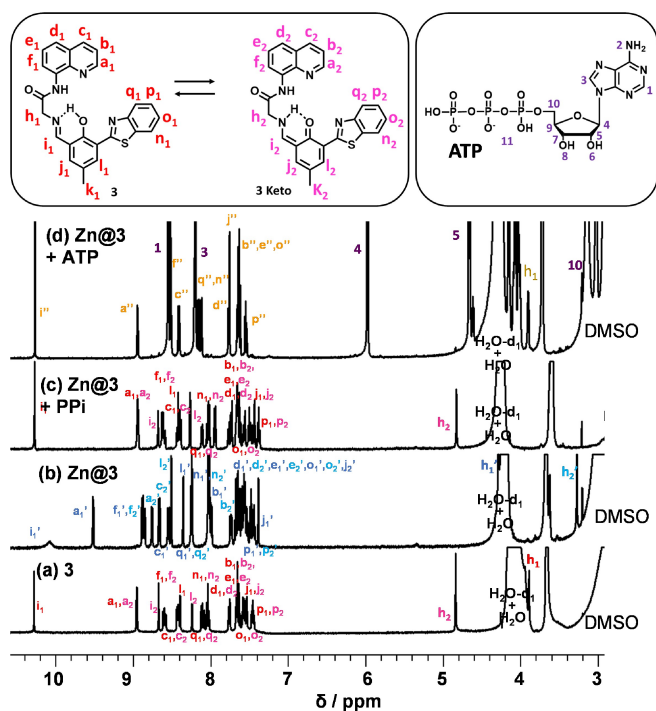


Figure 7. ^1H NMR spectra of **3** in the absence (a) of and in the presence of zinc(II) ion (b). ^1H NMR spectra of **3** in the presence of zinc(II) upon addition of PPI (c) and ATP (d). Conditions: $[\mathbf{3}] = 1.00\text{ mM}$, $[\text{zinc(II)}] = 1.25\text{ mM}$, $[\text{PPI}] = 3.00\text{ mM}$, $[\text{ATP}] = 3.00\text{ mM}$ in $\text{DMSO}-d_6$; HEPES (20 mM, $\text{pD} = 7$) = 3:1 (v:v).

Further, ^1H NMR spectra of **Zn@1–Zn@3** in the presence of ATP and PPI were recorded. Figures 5–7 show changes in chemical shifts of **1–3** associated with the removal of zinc(II) from the complex during the recognition processes. However, the **Zn@3** showed a slightly different behavior. The NMR data of **Zn@3 + PPI** indicate removal of Zn^{2+} from **Zn@3**, whereas in the NMR spectra of **Zn@3 + ATP** the signal pattern arising from ligand **3** was more simplified. Considering that the NMR data of **3 + ATP** is fully consistent with that of **Zn@3 + ATP**, it suggests that an ensemble composed of **3** (imine form) and ATP may have been formed after ATP was added to the **Zn@3** solution (see S43).

Fluorescence responses of the ensembles to anions

The previously described zinc(II) complexes were used to sense phosphate-related anions. Here, the addition of phosphate ions to the **Zn@1–Zn@3** leads to the formation of a new complex, or a subsequent removal of zinc(II) from the complex, which leads to dramatic changes of the optical properties. So far, the sensing mechanism utilizing removal of the zinc(II) from a dye complex has led to a relatively low sensitivity. Here, we show that this recognition mechanism in conjunction with fluorescent ligands allows for the discrimination of phosphate ions with high sensitivity and may be used in fluorescence-based sensor arrays.

Thus, fluorescence responses of **Zn@1–Zn@3** to anions were investigated (Figure 8 and S28–S42). In addition to ATP, ADP, AMP, PPI, and Pi, other anions including chloride, bromide, sulfate, nitrate, cyanide, and acetate were also examined. The anions were added to **Zn@1–Zn@3** ($5.0\text{ }\mu\text{M}$) in a HEPES buffer solution (10 mM, $\text{pH} = 7.0$) containing acetonitrile (50%, v/v). The efficient complexation between the ligands **1–3** and zinc(II) ensures that almost no free zinc(II) is present in the solution. This is important because free zinc(II) could bind to the analyte rather than metal centers in the complexes. Figure 8 shows typical fluorescence titration spectra of the ensembles **Zn@1–Zn@3** with phosphate ions. Specifically, **Zn@1–Zn@3** showed significant fluorescence responses to ATP, ADP, PPI, and Pi while the additions of the other anions led to negligible changes. The additions of phosphate ions reversed the zinc(II)-induced spectral changes, suggesting the removal of zinc(II) ion from the ensembles.

Saturation curves of the observed fluorescence responses upon the removal of zinc(II) ions from the ensembles allowed us to quantify the apparent binding affinity of these phosphate ions to the zinc(II) centers as a 1:1 stoichiometric process (Table 1). The apparent binding constants of **Zn@1** with phosphate ions follow the order of $\text{PPI} > \text{ATP} > \text{ADP} \gg \text{Pi} > \text{AMP}$, which corresponds to the order of the intrinsic binding affinity of zinc(II) toward these phosphate anions. In contrast to **Zn@1**, **Zn@2** and **Zn@3** show the binding affinities in the order of $\text{ATP} > \text{PPI} > \text{ADP} \gg \text{Pi} > \text{AMP}$.

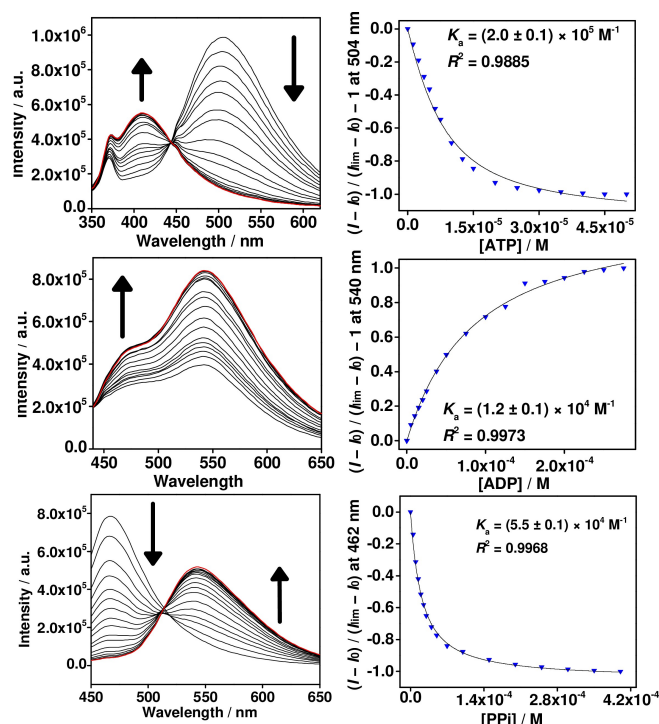


Figure 8. Top: Fluorescence titration spectra of **Zn@1** ($[\mathbf{1}] = 5.0\text{ }\mu\text{M}$, $[\text{zinc(II)}] = 5.0\text{ }\mu\text{M}$) upon addition of ATP ($\lambda_{\text{ex}} = 330\text{ nm}$). Center: Fluorescence titration spectra of **Zn@2** ($[\mathbf{2}] = 5.0\text{ }\mu\text{M}$, $[\text{zinc(II)}] = 5.0\text{ }\mu\text{M}$) upon addition of ADP ($\lambda_{\text{ex}} = 345\text{ nm}$). Bottom: Fluorescence titration spectra of **Zn@3** ($[\mathbf{3}] = 5.0\text{ }\mu\text{M}$, $[\text{zinc(II)}] = 5.0\text{ }\mu\text{M}$) upon addition of PPI ($\lambda_{\text{ex}} = 435\text{ nm}$).

Table 1. Apparent binding constants K ($\times 10^4 \text{ M}^{-1}$) of phosphate anions for the zinc(II) centers of Zn@1–Zn@3 ($[1-3] = 5.0 \mu\text{M}$, $[\text{zinc(II) nitrate}] = 5.0 \mu\text{M}$) with 5'-adenosine nucleotides, PPI, and Pi.^[a]

	Apparent affinity constants $\times 10^4 \text{ [M}^{-1}]$				
	ATP	ADP	AMP	PPI	Pi
Zn@1	19.6 \pm 1.0	4.5 \pm 0.1	NR	41.0 \pm 1.0	ND
Zn@2	9.3 \pm 0.3	1.2 \pm 0.1	NR	6.9 \pm 0.1	ND
Zn@3	12.0 \pm 0.1	1.1 \pm 0.1	NR	5.5 \pm 0.1	NR

[a] All titrations were performed in HEPES buffer (10 mM, pH=7) containing acetonitrile (50%, v/v). The K values were calculated based on the change in fluorescence intensity upon the addition of each phosphate anion. ND: Multiple equilibria appear to be involved, precluding calculation of the binding constant; NR: No appreciable response was observed.

The presence of the benzothiazole moieties and the corresponding hydrophobic environment around the zinc(II) centers in Zn@2 and Zn@3 results in decreased affinity for PPI. The observed fluorescence responses were well supported by the corresponding UV-vis absorption titrations (Figures S48–S59). It is noteworthy that Zn@2 and Zn@3 exhibited different response selectivity toward ATP and PPI compared to Zn@1 because such a different selectivity pattern could play an important role in the discrimination of anionic analytes using sensor arrays where the individual sensor contributions are analyzed by machine learning algorithms.^[29]

Sensing of adenine nucleotides using a sensor array

The different affinity order in the otherwise cross-reactive responses of Zn@1–Zn@3 toward phosphate anions suggests that the use of Zn@1–Zn@3 in a sensor array would lead to significant differences in the response patterns between ATP, ADP, and PPI as well as other phosphate anions. Thus, a fluorescence chemosensor array of Zn@1–Zn@3 was performed as follows: First, the solutions of ensembles ($[1-3] = 5.0 \mu\text{M}$, $[\text{zinc(II)}] = 5.0 \mu\text{M}$) in a HEPES buffer (pH 7, 10 mM) containing acetonitrile (50%, v/v) were dispensed into a 384-well microplate. Then, solutions of anions were added, and the fluorescence intensity of the resulting solutions was recorded using a microplate reader. The collected values of the fluorescence intensities were analyzed by linear discriminant analysis (LDA).^[29] Due to the strong selectivity bias of the Zn@1–Zn@3 toward phosphate anions the three ensembles Zn@1–Zn@3 allowed for distinguishing ATP, ADP, PPI, and Pi from 8 other analytes with 100% correct classification. The graphical output of the LDA shows separate clustering of ATP, ADP, PPI, and Pi from AMP and the other anions (Figure 9). The obtained results, namely the distance of the clusters from the control, are clearly in agreement with the order of the apparent affinity constants shown in Table 1.

The successful discrimination of ATP, ADP, PPI, and Pi prompted us to explore the utility of this array in the quantitative analysis of ATP. First, fluorescence patterns of the ensembles in the presence of different concentrations of ATP were investigated. The graphical output of the LDA showed

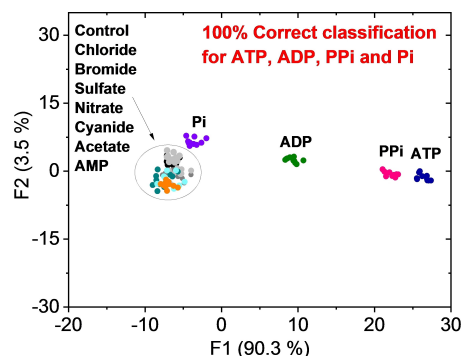


Figure 9. Graphical output of the qualitative linear discriminant analysis (LDA) from the response pattern of the ensembles Zn@1–Zn@3 to 11 individual analytes in HEPES buffer (pH 7, 10 mM) containing acetonitrile (50%, v/v). Clear clustering of ATP, ADP, PPI, and Pi is observed with 100% correct classification.

that the change in the concentration of ATP led to a differential response pattern of the fluorescent ensembles in the array (Figure 10). Excellent separation of the clusters corresponding to different ATP concentrations together with the smooth curved isotherm-resembling trajectory of the observed positions of the clusters suggests that the concentrations of ATP in unknown samples can be predicted using this sensor array. To achieve the prediction of the concentration of ATP in unknown samples, a support vector machine (SVM) based linear regression was employed. In this experiment, six data points with different concentrations of ATP ($[\text{ATP}] = 0, 10, 30, 40, 80,$ and $100 \mu\text{M}$) were used as known concentrations for calibration and two data points ($[\text{ATP}] = 20$ and $60 \mu\text{M}$) were analyzed as unknown concentrations. The SVM analysis predicted the two data points with a root mean square errors of the prediction (RMSEP) less than 2.5% (Figure 11). Thus far, to the best of our knowledge, this fluorescence chemosensor array recognizes the lowest ATP concentration (20 μM). The sensitive quantification of ATP with the high discrimination capability of the sensor

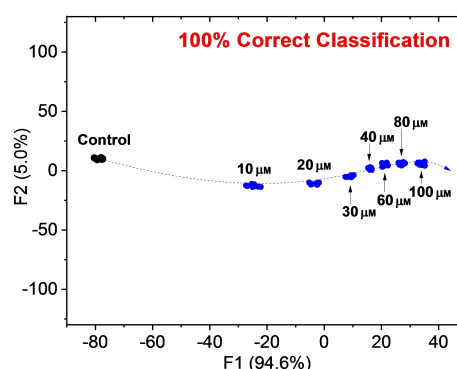


Figure 10. Graphical output of the LDA of the response pattern from the sensor array of ensembles Zn@1–Zn@3 toward ATP at different concentrations ($[\text{ATP}] = 0, 10, 20, 30, 40, 60, 80,$ and $100 \mu\text{M}$). Each clustering was identified with 100% correct classification in HEPES buffer (pH 7, 10 mM) containing acetonitrile (50%, v/v).

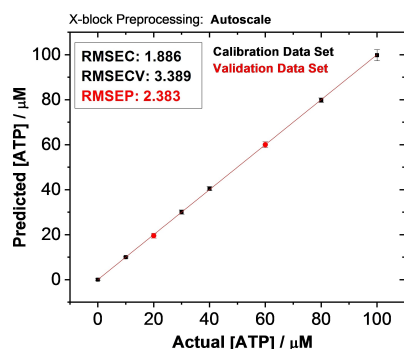


Figure 11. Prediction of the concentrations of ATP ([ATP] = 20 and 60 μM , red dots) by a machine learning algorithm (support vector machine) using six data points with different concentrations of ATP ([ATP] = 0, 10, 30, 40, 80, and 100 μM) as calibration data (black dots).

array illustrates the potential for the use of the present ensembles in sensor arrays aimed at quantitation of low levels of ATP.

Conclusion

In summary, fluorescent carboxyamidoquinoline receptors 1–3 comprising appended phenol (1) and hydroxyphenyl benzothiazole moieties (2 and 3) were synthesized as potential sensors for anions. The addition of zinc(II) to 1–3 led to the formation of the fluorescent ensembles (Zn@1–Zn@3). Here, the phosphate analytes are capable of removing zinc(II) from the ensemble, a process associated with dramatic changes in the spectroscopic properties of the sensing system. Thus, the response behavior of Zn@1–Zn@3 to various phosphate anions as well as other inorganic anions were investigated by means of fluorescence and NMR spectroscopy. Interestingly, we found that the ensembles showed significant fluorescence responses to multiposphates such as ATP, ADP, and PPI, and substantially lower response to AMP and Pi. This suggests that the larger number of phosphate moieties within the analyte molecule results in a stronger interaction with Zn(II) causing the removal of the zinc (II) from the complex. Solutions of Zn@1–Zn@3 were used in a sensor array where the resulting response patterns to anions allowed for the discrimination of ATP, ADP, PPI, and Pi from other anions. Furthermore, the quantitative regression analysis led to the prediction of the concentrations of ATP in unknown samples with high sensitivity. These results illustrate the potential utility of the present carboxyamidoquinoline-based zinc(II) ensembles as components of sensor arrays for the quantitative detection of low levels of phosphates in biological fluids such as urine and saliva.

Experimental Section

General

NMR spectra were taken by a Bruker Avance 500 MHz NMR spectrometer. In ^1H and ^{13}C NMR measurements, chemical shifts (δ) are reported downfield from the chemical shift of tetramethylsilane as an internal standard. Mass spectrometry (MS) was performed by using a fast atom bombardment (FAB) mass spectrometer (JEOL JMS-700) and an atmospheric pressure chemical ionization (APCI) and electrospray ionization (ESI) mass spectrometer (Bruker micrOTOF). *m*-Nitrobenzylalcohol was used as a matrix for FAB-MS and Tuning-Mix was used as a calibration standard for APCI and ESI-MS. Elemental analyses were performed on an Exeter Analytical, Inc. CE-440F elemental analyzer. The absorption and fluorescence spectra were measured using an Agilent Technologies Cary 60, a JASCO FP-6300 spectrophotometer and Edinburg spectrofluorimeter FLSP 920, respectively.

Materials

Reagents used for the synthesis were commercially available and used as supplied. Dry dichloromethane and tetrahydrofuran were prepared according to standard procedures. The syntheses of 2-amino-*N*-(quinolin-8-yl) acetamide^[30] and 2-(benzo[d]thiazol-2-yl)-4-methylphenol^[31] were performed according to the reported procedures. The synthesis of 3-(benzo[d]thiazol-2-yl)-2-hydroxy-5-methylbenzaldehyde is described in the Supporting Information.

Synthesis

Synthesis of 2-((2-hydroxybenzyl)amino)-*N*-(quinolin-8-yl) acetamide (1)

2-Amino-*N*-(quinolin-8-yl) acetamide (0.96 g, 3.4 mmol) and salicylaldehyde (0.41 mL, 3.9 mmol) were dissolved in dry ethanol (60 mL), and the solution was stirred for 6 h at room temperature. The mixture was then cooled to 0 $^{\circ}\text{C}$, and sodium borohydride (0.31 g, 9.0 mmol) in dry ethanol (50 mL) was added to the mixture. The resulting mixture was allowed to stir at room temperature under a nitrogen atmosphere for 4 h. The reaction mixture was poured into 0.1 M hydrochloric acid (20 mL) and then ethyl acetate (150 mL) was added to the aqueous mixture. The organic layer was separated and dried over sodium sulfate. After evaporation of the filtrate *in vacuo*, the residue was recrystallized from ethyl acetate to give 0.48 g of 1 as a white solid in 45% yield. ^1H NMR (500 MHz, CDCl_3) δ (ppm): 10.04 (s, 1H), 8.80 (dd, J = 4.20; 1.65 Hz, 1H), 8.76 (dd, J = 6.60; 2.20 Hz, 1H), 8.18 (dd, J = 1.65; 8.23 Hz, 1H), 7.58–7.54 (m, 2H), 7.47 (dd, J = 4.25; 8.30 Hz, 1H), 7.21 (td, J = 1.43; 7.75 Hz, 1H), 7.04 (d, J = 7.45 Hz, 1H), 6.90 (dd, J = 8.10; 0.90 Hz, 1H), 6.81 (td, J = 7.40; 1.10 Hz, 1H), 4.11 (s, 2H), 3.64 (s, 2H). ^{13}C NMR (126 MHz, CDCl_3) δ (ppm): 168.6, 157.85, 148.41, 138.32, 136.4, 133.79, 129.11, 129.05, 127.97, 127.33, 122.16, 122.02, 121.79, 119.39, 116.69, 116.63, 52.29, 51.67. FAB-MS: m/z = 308 $[\text{M} + \text{H}]^+$. Elemental analysis calcd (%) for $\text{C}_{18}\text{H}_{17}\text{N}_3\text{O}_2$: C 70.34, H 5.58, N 13.67; found: C 70.04, H 5.54; N 13.44.

Synthesis of 2-((3-(benzo[d]thiazol-2-yl)-2-hydroxy-5-methylbenzyl)amino)-*N*-(quinolin-8-yl) acetamide (2)

2-Amino-*N*-(quinolin-8-yl) acetamide (0.41 g, 1.5 mmol) and 3-(benzo[d]thiazol-2-yl)-2-hydroxy-5-methylbenzaldehyde (0.31 g, 1.5 mmol) were dissolved in dry ethanol (60 mL), and the solution

was refluxed at 80 °C for 2 h under a nitrogen atmosphere. The mixture was cooled to 0 °C, and sodium borohydride (0.23 g, 6.1 mmol) in dry ethanol (30 mL) was added to the mixture. Then the mixture was allowed to stir at room temperature for 2 h under a nitrogen atmosphere. The resulting mixture was poured into 0.1 M hydrochloric acid (10 mL) and ethyl acetate (100 mL) was added to the aqueous mixture. The organic layer was dried over sodium sulfate. After evaporation of the filtrate *in vacuo*, recrystallization of the residue from ethyl acetate afford 0.45 g of **2** as a light yellow solid in 66% yield. ¹H NMR (500 MHz, CDCl₃) δ (ppm): 12.69 (s, 1H), 11.47 (s, 1H), 8.83–8.85 (m, 2H), 8.25 (dd, *J*=8.20; 1.65 Hz, 1H), 7.93 (dd, *J*=17.05; 7.95 Hz, 1H), 7.49–7.56 (m, 3H), 7.39–7.43 (m, 3H), 7.30 (s, 1H), 4.05 (s, 2H), 3.59 (s, 2H), 2.56 (s, 1H), 2.35 (s, 3H). ¹³C NMR (126 MHz, CDCl₃): δ (ppm) 170.7, 169.4, 154.3, 151.8, 148.5, 139.1, 136.1, 134.6, 134.6, 132.7, 128.3, 128.1, 127.6, 127.5, 127.3, 126.7, 125.5, 122.1, 121.6, 121.5, 121.4, 116.6, 116.3, 52.9, 49.4, 20.5. FAB-MS: *m/z*=455 [M+H]⁺. Elemental analysis: calcd (%) for C₂₆H₂₂N₄O₂S : C 68.70, H 4.88, N 12.33; found: C 68.64, H 4.93, N 12.27.

Synthesis of (Z)-2-((3-(benzo[d]thiazol-2-yl)-2-hydroxy-5-methylbenzyl)imino)-N-(quinolin-8-yl)acetamide (**3**)

2-Amino-N-(quinolin-8-yl) acetamide (0.15 g, 0.74 mmol) and 3-(benzo[d]thiazol-2-yl)-2-hydroxy-5-methylbenzaldehyde (0.20 g, 0.74 mmol) were dissolved in dry ethanol (50 mL), and the solution was refluxed at 80 °C under a nitrogen atmosphere for 3 h. After cooling to room temperature, a yellowish precipitate was collected to give 0.29 g of **3** as a yellow solid in 87% yield. ¹H NMR (500 MHz, CDCl₃) δ (ppm): 12.69 (s, 1H), 11.47 (s, 1H), 8.83–8.85 (m, 2H), 8.13 (d, *J*=8.20 Hz, 1H), 7.97 (d, *J*=7.75 Hz, 1H), 7.80 (s, 1H), 7.52–7.58 (m, 3H), 7.41–7.46 (m, 3H), 4.64 (s, 1H), 2.49 (s, 3H). ¹³C NMR (126 MHz, CDCl₃): δ (ppm) 167.7, 156.7, 151.9, 148.5, 138.8, 136.2, 134.6, 134.1, 133.4, 132.6, 128.6, 128.6, 127.3, 126.4, 125.2, 122.5, 121.9, 121.7, 121.5, 121.2, 119.6, 116.5, 111.1, 77.7, 63.6, 63.5. APCI-MS: *m/z*=453 [M+H]⁺. Elemental analysis calcd (%) for C₂₆H₂₀N₄O₂S : C, 69.01, H 4.45, N 12.38; found: C 68.81, H 4.45, N 12.36.

Preparation of sensor arrays

The sensor array experiments were performed in a 384-well plate. Solutions of Zn@1–Zn@3 ([1–3]=5 μM, [zinc(II) nitrate]=5 μM) in the absence and the presence of anions were prepared in HEPES buffer (pH=7, 10 mM) containing acetonitrile (50%, v/v). The solutions (100 μL) were then injected into the wells of the 384-well plate using a Bio Nex Nanodrop (BNX Nanodrop Express) dispenser. The fluorescence changes obtained from the solutions were recorded by a BMG CLARIO star microplate reader (Zn@1: λ_{ex}/λ_{em}=330 nm/410 nm and 330 nm/504 nm, Zn@2: λ_{ex}/λ_{em}=345 nm/471 nm and 345 nm/545 nm, Zn@3: λ_{ex}/λ_{em}=434 nm/465 nm and 434 nm/558 nm). Each experiment was performed in 12 repetitions. The resulting fluorescence patterns were analyzed using LDA. Quantitative analysis of ATP was performed using Eigenvector SVM software package SOLO.

Acknowledgements

This work was supported by the Bowling Green State University (Building Strength Award, Project no. 33000211). This work was also supported by JSPS KAKENHI Grant Numbers JP18 K05088 and JP19H02704.

Conflict of Interest

The authors declare no conflict of interest.

Keywords: chemosensors · sensor arrays · pattern recognition · nucleotide triphosphate · fluorescence

- [1] a) J. L. Sessler, P. A. Gale, W. S. Cho, *Anion Receptor Chemistry*, Royal Society Of Chemistry, **2006**; b) A. Bianchi, K. Bowman-James, E. Garcia-España, *Supramolecular Chemistry of Anions*, Wiley-VCH, New York, NY, **1997**.
- [2] a) N. Busschaert, C. Caltagirone, W. Van Rossom, P. A. Gale, *Chem. Rev.* **2015**, *115*, 8038–8155; b) P. A. Gale, C. Caltagirone, *Chem. Soc. Rev.* **2015**, *44*, 4212–4227; c) S. Pal, T. K. Ghosh, R. Ghosh, S. Mondal, P. Ghosh, *Coord. Chem. Rev.* **2020**, *405*, 213128.
- [3] R. L. P. Adams, J. T. Knowler and D. P. Leader, *The biochemistry of the nucleic acids*, Chapman and Hall, 10th edn., **1986**.
- [4] E. Buxbaum, *Fundamentals of Protein Structure and Function*, Springer International Publishing, **2015**; b) R. L. Khandelwal, J. H. Wang, *Reversible Protein Phosphorylation in Cell Regulation*, Springer US, **1993**.
- [5] J. J. Feher, *Quantitative Human Physiology: An Introduction*, Academic Press, Boston, **2017**.
- [6] D. E. C. Corbridge, *Phosphorus: Chemistry, Biochemistry and Technology*, CRC Press, 6th edn., **2016**.
- [7] P. J. A. Kleinman, A. N. Sharpley, R. W. McDowell, D. N. Flaten, A. R. Buda, L. Tao, L. Bergstrom, Q. Zhu, *Plant Soil* **2011**, *349*, 169–182.
- [8] a) J. R. Knowles, *Annu. Rev. Biochem.* **1980**, *49*, 877–919; b) F. M. Ashcroft, F. M. Gribble, *Diabetologia* **1999**, *42*, 903–919; c) S. Przedborski, M. Vila, *Clin. Neurosci. Res.* **2001**, *1*, 407–418; d) S. M. Cardoso, I. Santana, R. H. Swerdlow, C. R. Oliveira, *J. Neurochem.* **2004**, *89*, 1417–1426; e) A. V. Gourine, E. Llaudet, N. Dale, K. M. Spyer, *Nature* **2005**, *436*, 108–111; f) G. Burnstock, *Trends Pharmacol. Sci.* **2006**, *27*, 166–176; g) P. Bhargava, R. G. Schnellmann, *Nat. Rev. Nephrol.* **2017**, *13*, 629–646.
- [9] a) P. Yeung, L. Ding, W. L. Casley, *J. Pharm. Biomed. Anal.* **2008**, *47*, 377–382; b) A. V. Akhova, A. G. Tkachenko, *Acta Chromatogr.* **2019**, *31*, 45–48.
- [10] a) M. W. Griffiths, *J. Dairy Sci.* **1993**, *76*, 3118–3125; b) C. Zhang, Z. H. Wei, B. C. Ye, *Biotechnol. J.* **2013**, *8*, 1280–1291; c) C. Ma, C. Lin, Y. Wang, X. Chen, *TrAC Trends Anal. Chem.* **2016**, *77*, 226–1241; d) G. Morciano, A. C. Sarti, S. Marchi, S. Missiroli, S. Falzoni, L. Raffaghello, V. Pistoia, C. Giorgi, F. D. Virgilio, P. Pinton, *Nat. Protoc.* **2017**, *12*, 1542–1562; e) F. Gallez, M. Fadel, O. Scruel, F. Cantraine, P. Courtois, *Cell Biochem. Funct.* **2000**, *18*, 103–108.
- [11] a) T. Sakamoto, A. Ojida, I. Hamachi, *Chem. Commun.* **2009**, *0*, 141–152; b) Y. Zhou, Z. Xu, J. Yoon, *Chem. Soc. Rev.* **2011**, *40*, 2222–2235; c) A. E. Hargrove, S. Nieto, T. Zhang, J. L. Sessler, E. V. Anslyn, *Chem. Rev.* **2011**, *111*, 6603–6782; d) H. T. Ngo, K. A. Liu, K. A. Jolliffe, *Chem. Soc. Rev.* **2012**, *41*, 4928–4965; e) J. Wu, B. Kwon, W. Liu, E. V. Anslyn, P. Wang, J. S. Kim, *Chem. Rev.* **2015**, *115*, 7893–7943; f) Y. Wu, J. Wen, H. J. Li, S. G. Sun, Y. Q. Xu, *Chin. Chem. Lett.* **2017**, *28*, 1916–1924; g) A. M. Agafontsev, A. Ravi, T. A. Shumilova, A. Oshchepkov, E. A. Kataev, *Chem. Eur. J.* **2018**, *25*, 2684–2694.
- [12] a) S. E. Schneider, S. N. O’Nei, E. V. Anslyn, *J. Am. Chem. Soc.* **2000**, *122*, 542–543; b) C. Li, M. Numata, M. Takeuchi, S. Shinkai, *Angew. Chem. Int. Ed.* **2005**, *44*, 6371–6374; *Angew. Chem.* **2005**, *117*, 6529–6532; c) H. Wang, W. H. Chan, *Org. Biomol. Chem.* **2008**, *6*, 162–168; d) P. S. Sharma, M. Dabrowski, K. Noworyta, T. P. Huynh, C. B. Kc, J. W. Sobczak, P. Pieta, F. D’Souza, W. Kutner, *Anal. Chim. Acta* **2014**, *844*, 61–69; e) T. Ema, K. Okuda, S. Watanabe, T. Yamasaki, T. Minami, N. A. Esipenko, P. Anzenbacher Jr., *Org. Lett.* **2014**, *16*, 1302–1305; f) A. Akdeniz, M. G. Caglayan, I. Polivina, P. Anzenbacher Jr., *Org. Biomol. Chem.* **2016**, *14*, 7459–7462; g) O. Sunnapu, N. G. Kotla, B. Maddiboyina, S. Marepally, J. Shanmugapriya, K. Sekar, S. Singaravadevel, G. Sivaraman, *ChemistrySelect* **2017**, *2*, 7654–7658; h) K. Y. Tan, C. Y. Li, Y. F. Li, J. Fei, B. Yang, Y. J. Fu, F. Li, *Anal. Chem.* **2017**, *89*, 1749–175; i) S. Farshbaf, P. Anzenbacher Jr., *Chem. Commun.* **2019**, *55*, 1770–1773.
- [13] a) P. Anzenbacher Jr., P. Lubal, P. Bucek, M. A. Palacios, M. E. Kozelkova, *Chem. Soc. Rev.* **2010**, *39*, 3954–3979; b) D. G. Smith, I. L. Topolnicki, V. E. Zwicker, K. A. Jolliffe, E. J. New, *Analyst* **2017**, *142*, 3549–3563; c) Z. Li, J. R. Askim, K. S. Suslick, *Chem. Rev.* **2019**, *119*, 231–292; d) Y. Geng, W. J. Peveler, V. M. Rotello, *Angew. Chem. Int. Ed.* **2019**, *58*, 5190–5200; *Angew. Chem.* **2019**, *131*, 5244–5255.

- [14] a) M. Sc, G. Mj, S. Se, M. Jt, A. Ev, *J. Am. Chem. Soc.* **2003**, *125*, 1114–1115; b) A. Buryak, A. Pozdnoukhov, K. Severin, *Chem. Commun.* **2007**, *23*, 2366–2368; c) Z. Yao, X. Feng, Hong, W. C. Li, G. Shi, *Chem. Commun.* **2009**, *31*, 4696–4698; d) V. Hamedpour, Y. Sasaki, Z. Zhang, R. Kubota, T. Minami, *Anal. Chem.* **2019**, *91*, 13627–13632.
- [15] a) F. Zaubitzer, A. Buryak, K. Severin, *Chem. Eur. J.* **2006**, *12*, 3928–3934; b) S. H. Lim, C. J. Musto, E. Park, W. Zhong, K. S. Suslick, *Org. Lett.* **2008**, *10*, 4405–4408; c) C. J. Musto, S. H. Lim, K. S. Suslick, *Anal. Chem.* **2009**, *81*, 6526–6533.
- [16] a) A. T. Wright, E. V. Anslyn, J. T. McDevitt, *J. Am. Chem. Soc.* **2005**, *127*, 17405–17411; b) A. Buryak, K. Severin, *Angew. Chem. Int. Ed.* **2005**, *44*, 7935–7938; *Angew. Chem.* **2005**, *117*, 8149–8152; c) S. Rochat, J. Gao, X. Qian, F. Zaubitzer, K. Severin, *Chem. Eur. J.* **2010**, *16*, 104–113; d) E. G. Shcherbakova, V. Brega, T. Minami, S. Sheykhi, T. D. James, *Chem. Eur. J.* **2016**, *22*, 10074–10080; e) B. Wang, J. Han, C. Ma, M. Bender, K. Seehafer, A. Herrmann, U. H. F. Bunz, *Chem. Eur. J.* **2017**, *23*, 12471–12474; f) F. Octa-Smolín, J. Niemeyer, *Chem. Eur. J.* **2018**, *24*, 16506–6510; g) B. Wang, J. Han, N. M. Bojanowski, M. Bender, C. Ma, K. Seehafer, A. Herrmann, U. H. F. Bunz, *ACS Sens.* **2018**, *3*, 1562–1568.
- [17] a) A. T. Wright, M. J. Griffin, Z. Zhong, S. C. McCleskey, E. V. Anslyn, J. T. McDevitt, *Angew. Chem.* **2005**, *117*, 6533–6536; b) H. C. Zhou, L. Baldini, J. Hong, A. J. Wilson, A. D. Hamilton, *J. Am. Chem. Soc.* **2006**, *128*, 2421–2425; c) C. C. You, O. R. Miranda, B. Gider, P. S. Ghosh, I. B. Kim, B. Erdogan, S. A. Krovi, U. H. F. Bunz, V. M. Rotello, *Nat. Nanotechnol.* **2007**, *2*, 318–323; d) P. Behera, M. De, *Chem. Asian J.* **2019**, *14*, 553–560.
- [18] a) T. Mayr, C. Igel, G. Liebsch, I. Klimant, O. S. Wolfbeis, *Anal. Chem.* **2003**, *75*, 4389–4396; b) H. S. Hewage, E. V. Anslyn, *J. Am. Chem. Soc.* **2009**, *131*, 13099–13106; c) L. H. Yuen, R. M. Franzini, S. L. Wang, P. Crisalli, V. Singh, W. Jiang, E. T. Kool, *Angew. Chem. Int. Ed.* **2014**, *53*, 5361–5365; *Angew. Chem.* **2014**, *126*, 5465–5469; d) H. Qiu, F. Pu, X. Ran, J. S. Ren, X. G. Qu, *Chem. Eur. J.* **2017**, *23*, 9258–9261.
- [19] a) N. A. Rakow, K. S. Suslick, *Nature* **2000**, *406*, 710–713; b) C. Zhang, K. S. Suslick, *J. Am. Chem. Soc.* **2005**, *127*, 11548–11549; c) Y. Liu, T. Minami, R. Nishiyabu, Z. Wang, P. Anzenbacher Jr., *J. Am. Chem. Soc.* **2013**, *135*, 7705–7712; d) P. Anzenbacher Jr., Y. L. Liu, M. A. Palacios, T. Minami, Z. Wang, R. Nishiyabu, *Chem. Eur. J.* **2013**, *19*, 8497–8506; e) Y. Liu, M. Bonizzoni, *J. Am. Chem. Soc.* **2014**, *136*, 14223–14229; f) F. Octa-Smolín, J. Niemeyer, *Chem. Eur. J.* **2018**, *24*, 16506–16510; g) Y. Qi, W. Xu, R. Kang, N. Ding, Y. Wang, G. He, Y. Fang, *Chem. Sci.* **2018**, *9*, 1892–1901; h) M. Pushina, P. Koutnik, R. Nishiyabu, T. Minami, P. Savechenkov, P. Anzenbacher Jr., *Chem. Eur. J.* **2018**, *24*, 4879–4884; i) G. V. Zyryanov, M. A. Palacios, P. Anzenbacher Jr., *Angew. Chem.* **2007**, *119*, 7995–7998.
- [20] a) R. Nishiyabu, M. A. Palacios, W. Dehaen, P. Anzenbacher Jr., *J. Am. Chem. Soc.* **2006**, *128*, 11496–11504; b) M. A. Palacios, R. Nishiyabu, M. Marquez, P. Anzenbacher Jr., *J. Am. Chem. Soc.* **2007**, *129*, 7538–7544; c) A. D. Hughes, I. C. Glenn, A. D. Patrick, A. Ellington, E. V. Anslyn, *Chem. Eur. J.* **2008**, *14*, 1822–1827; d) L. Mosca, S. K. Behzad, P. Anzenbacher Jr., *J. Am. Chem. Soc.* **2015**, *137*, 7967–7969; e) D. G. Smith, I. L. Topolnicki, V. E. Zwicker, K. A. Jolliffe, E. J. New, *Analyst* **2017**, *142*, 3549–3563.
- [21] a) T. Minami, F. Emami, R. Nishiyabu, Y. Kubo, P. Anzenbacher Jr., *Chem. Commun.* **2016**, *52*, 7838–7841; b) S. Hu, X. Li, K. Wang, Q. Wu, G. Zhang, X. Liu, *Sens. Actuators B* **2020**, *310*, 127851; c) W. Miao, L. Wang, Q. Liu, S. Guo, L. Zhao, J. Peng, *Chem. Asian J.* **2021**, *16*, 247–251.
- [22] a) Y. W. Choi, J. J. Lee, C. Kim, *RSC Adv.* **2015**, *5*, 60796–60803; b) K. Boonkitpatarakul, A. Smata, K. Kongnukool, S. Srisurichan, K. Chainok, M. Sukwattanasinitt, *J. Lumin.* **2018**, *198*, 59–67; c) Z. Dong, X. Le, P. Zhou, C. Dong, J. Ma, *New J. Chem.* **2014**, *38*, 1802–1808; d) E. J. Song, J. Kang, G. R. You, G. J. Park, Y. Kim, S.-J. Kim, C. Kim, R. G. Harrison, *Dalton Trans.* **2013**, *42*, 15514–15520.
- [23] a) Y. S. Santos, E. Ramasamy, V. Ramamurthy, F. S. Rodembusch, *J. Mater. Chem. C* **2016**, *4*, 2820–2827; b) W. Meng, Z. Pei, Y. Wang, M. Sun, Q. Xu, J. Cen, K. Guo, K. Xiao, Z. Li, *J. Hazard. Mater.* **2021**, *410*, 124811; c) C. W. Ghanavatkar, V. R. Mishra, N. Sekar, E. Mathew, S. S. Thomas, I. H. Joe, *J. Mol. Struct.* **2020**, *1203*, 127401; d) S. M. Aly, A. Usman, M. AlZayer, G. A. Hamdi, E. Alarousu, O. F. Mohammed, *J. Phys. Chem. B* **2015**, *119*, 2596–2603.
- [25] a) Y. Zhang, X. Guo, W. Si, L. Jia, X. Qian, *Org. Lett.* **2008**, *10*, 473–476; b) Y. Chen, K.-Y. Han, Y. Liu, *Bioorg. Med. Chem.* **2007**, *15*, 4537–4542; c) H. Song, Z. Zhang, *Dyes Pigment.* **2019**, *165*, 172–181.
- [26] S. Das, S. Goswami, K. Aich, K. Ghoshal, C. K. Quah, M. Bhattacharyya, H. K. Fun, *New J. Chem.* **2015**, *39*, 8582–8587.
- [27] a) A. Gomathi, M. Vasanthi, P. Viswanthamurthi, S. Suresh, R. Nandhukumar, *ChemistrySelect* **2018**, *3*, 11809–11815; b) M. L. O'Duill, R. Matsuura, Y. Wang, J. L. Turnbull, J. A. Gurak, D. W. Gao, G. Lu, P. Liu, K. M. Engle, *J. Am. Chem. Soc.* **2017**, *139*, 15576–15579.
- [28] H. G. Lee, J. H. Lee, S. P. Jang, I. H. Hwang, S. J. Kim, Y. Kim, C. Kim, R. G. Harrison, *Inorg. Chim. Acta* **2013**, *394*, 542–551.
- [29] a) S. Stewart, M. Adams Ivy, E. V. Anslyn, *Chem. Soc. Rev.* **2014**, *43*, 70–84; b) A. T. Wright, E. V. Anslyn, *Chem. Soc. Rev.* **2006**, *35*, 14–28.
- [30] J. Zhang, X. Wang, C. Tu, J. Lin, J. Ding, L. Lin, Z. Wang, C. He, C. Yan, X. You, Z. Guo, *J. Med. Chem.* **2003**, *46*, 3502–3507.
- [31] J. Li, Y. Chen, T. Chen, J. Qiang, Z. Zhang, T. Wei, W. Zhang, F. Wang, X. Chen, *Sens. Actuators B* **2018**, *268*, 446–455.

Manuscript received: March 10, 2021

Accepted manuscript online: June 15, 2021

Version of record online: ■■■, ■■■■

FULL PAPER

Fluorescent carboxyamidoquinoline-zinc(II) assemblies were investigated as sensors for biologically relevant phosphate anions in water at low concentrations (micromolar). Analyte-specific changes in fluorescence allow for differentiation of inorganic phosphate, pyrophosphate, ADP, and ATP from eight other anionic analytes in a HEPES buffer. A fluorescence based array enabled quantitative analysis of ATP in the concentration range of 5–100 μM .



Dr. M. Pushina, S. Farshbaf, W. Mochida, M. Kanakubo, Dr. R. Nishiyabu, Prof. Dr. Y. Kubo, Prof. Dr. P. Anzenbacher, Jr.**

1 – 9

A Fluorescence Sensor Array Based on Zinc(II)-Carboxyamidoquinolines: Toward Quantitative Detection of ATP

